

Optimum influence of tensile functions on welded parts of AA 2024-T3 produced from friction stir mechanism utilizing air and water

Ghassan Shaker Abdul Ridha¹, Zaman Khalil Ibrahim², Mohammed Abdulridha Abbas^{3,4}, Ola Mohammed Merzah⁵

¹ Department of Electrical Techniques, Technical Institute Kut, Middle Technical University, Baghdad, Iraq

² Department of Power Mechanics Techniques, Technical Institute Kut, Middle Technical University, Baghdad, Iraq

³ Aeronautical Techniques Engineering Department, Engineering Technical College-Najaf, Al-Furat Al-Awsat Technical University (ATU), Najaf 54001, Iraq

⁴ Sustainable Manufacturing and Recycling Technology, Advanced Manufacturing and Materials Center (SMART-AMMC), Universiti Tun Hussein Onn Malaysia (UTHM), Parit Raja 86400, Malaysia

⁵ Air conditioning and Refrigeration Techniques Engineering Department, Al-Mustaqbal University College, Babylon 51001, Iraq

ABSTRACT

Friction Stir Welding (FSW) is a modern technology employed in welding aluminum alloys in various industrial fields such as airplane industries. Therefore, AA 2024-T3 alloy can be one of the active materials used in this field. From here, numerous studies have been conducted on the natural flow of air and water to cool the welded joints of this alloy. Nonetheless, the forced air and water were not utilized with this alloy. Hence, the purpose of this study is to apply these forced convection mechanisms to specify the optimal outputs of tensile functions using multi-objective optimization by the General Full Factorial (GFF) technique. In addition, the rotational speeds were 800, 1000, 1200 rpm in this experimental medium. Therefore, the optimal parameters resulting from this work were 1200 rpm and forced water to achieve the best performance. Furthermore, the morphology of the fracture region is induced by these parameters leading to appearing big dimples. Finally, these dimples contribute to enhancing the plastic fracture without brittleness.

Keywords: FSW, AA 2024-T3, Tensile strength, Fracture zone, General Full Factorial.

Corresponding Author:

Mohammed Abdulridha Abbas
Aeronautical Techniques Engineering Department
Engineering Technical College-Najaf, Al-Furat Al-Awsat Technical University (ATU)
Najaf 54001, Iraq
E-mail: mohd.a.abbas@atu.edu.iq

1. Introduction

It is no mystery the vital role of AA 2024-T3 alloy in the fields of airplane, aerospace, and aviation aircraft [1], [2]. The main reasons for employing this alloy are represented by high performance, good fatigue, lightweight, and corrosion resistance besides low cost. Accordingly, these properties have prompted the researchers to study the Friction Stir Welding (FSW) operation on this aluminum alloy as a promising mechanism [3], [4].

The strength and rotational speed are interesting points obtained from the prior studies of AA 2024-T3 alloy under the operation FSW. Therefore, these points have contributed to the feasibility of FSW by enhancing the life of welded specimens [5]. These outputs led to focusing on dealing with the tensile case to recognize the strength behavior. Consequently, this behavior has observably grown during the increase in rotational speed. Unfortunately, it is accompanied by this behavior dropping in the ductility of this specimen [6]. From here, these outcomes have proven the brittle of welded joints. Likewise, the elongation was boosted to 8.5%, while the ultimate tensile is 93.9% of un-welded AA 2024-T3 [7]. Thus, the side effects are associated with enhancing the strength property of welded joint [8]. The primary contributors to these effects were precarious grain size

depending on the increase in the rotation of tool speed. As a result, this speed caused the unsymmetrical distribution of residual stresses of the welded parts at the maximum applied tensile [9], [10]. Hence, tensile studies were unfortunate under the natural flow of air.

The authors strived to use other cooling options instead of natural airflow to enhance FSW operation. Therefore, there were trials by using types of materials instead of AA 2024-T3 alloy. As examples of these premises, Al5083 alloy under this operation has been upgraded through applying water cooling. This upgrade led to refining grain size and reducing the distributed temperature. Furthermore, both tensile ability and ductility were improved in this alloy [11]. These behaviors also appeared on AA 7075-T651 alloy, besides the increasing hardness and yield point concerning both forced air and water [12]. Therefore, these outcomes have stimulated researchers in the FSW field to develop the properties of the welded region of AA 2024-T3 alloy. Accordingly, the microhardness of AA 2024-T3 alloy has advanced by employing a natural flow of water compared to the microhardness of FSW operating with airflow. This feature was due to refining microstructure using this unique hybrid technique of this flow type with FSW [13]. Hence, the immersing of this alloy underwater raised the microhardness from 138.7 HV to 139.3 HV. In contrast, the peak temperature of this immersed alloy was dropped to 453.3 °C [14].

Depending on this brief survey, it turned out that the natural flow of water contributed to developing the welded region properties of AA2024-T3 samples, as compared to the un-forced air. In addition, the role of forced air and water in progressing the tensile, ductility, and yield point of AA 7075-T651 has been demonstrated. Accordingly, both forced air and water were not employed with the welded parts of AA2024-T3 in the FSW environment. Consequently, the present study aims to assign the tensile functions of welded components of AA 2024-T3 resulting from these forced flows. Moreover, the optimum output of parameters is selected using the Multi-Objective optimization based on the General-Full-Factorial (GFF) technique.

According to this context, the rotational speeds utilized in the current FSW mechanism are 800, 1000, and 1200 rpm. Furthermore, the forced flow is applied in this mechanism for both air and water, separately, besides the natural flow of air. Hence, these parameters' levels and this mechanism have been adopted to test a tensile of welded parts of AA 2024-T3. Therefore, it is essential to comprehend the functions of tensile results in the current study. Therefore, in the succeeding chapters: work materials, experimental conditions, designed trials, and an optimization technique are illustrated for exhibiting a concept of the accredited methodology to specify these functions.

2. Experimental medium and work materials

AA 2024-T3 alloy was employed as the work material's plates in the current study. Here, these plates were cut into two rectangular parts with dimensions (200×100×5) mm³, as demonstrated in Figure 1(C). The Friction-Stir-Welding (FSW) mechanism was performed by Semi-Automatic Vertical Milling Machine, India. As illustrated in Figure 1(a), the ejector nozzle has been applied on the FSW line at pressure 0.55 MPa for water and air. Besides, the machine's parameters utilized were 800, 1000, 1200 rpm, with 28 mm/min for rotational speed and feed rate, respectively. Meanwhile, the probe welding depicted in Figure 1(b) was installed as a tool in this machine to implement the mechanism of stir-welding by friction with these rectangular parts. This probe was made from water hardening tool steel, and the dimensions of this probe can be observed in Figure 1(b).

On the other hand, Scanning Electron Microscopy (SEM)/Energy Dispersive X-Ray Spectroscopy (EDS) model (Hitachi-SU1510, Japan) has been employed to specify the chemical composition of work materials: workpiece and Probe-Tool of welding. In addition, SEM/EDS was wielded to capture the micrographs of the fracture zone resulting from the tensile test. In Figure 2(a) and (b), the observed chemical composition was demonstrated as a royal bar for Workpiece: AA 2024-T3 and Welding Probe: Water Hardening Tool Steel-AISI-W1, respectively, depending on the EDS test. In contrast, the yellow bar indicated the standard of chemical composition to the over-mentioned work materials. According to the SEM's job, the FIJI program has been employed here, as a twin-integrated, to convert 2D-micrograph to 3D-topography [15]. This topography, as planned in results, contributes to clarifying the morphology of the fracture zone.

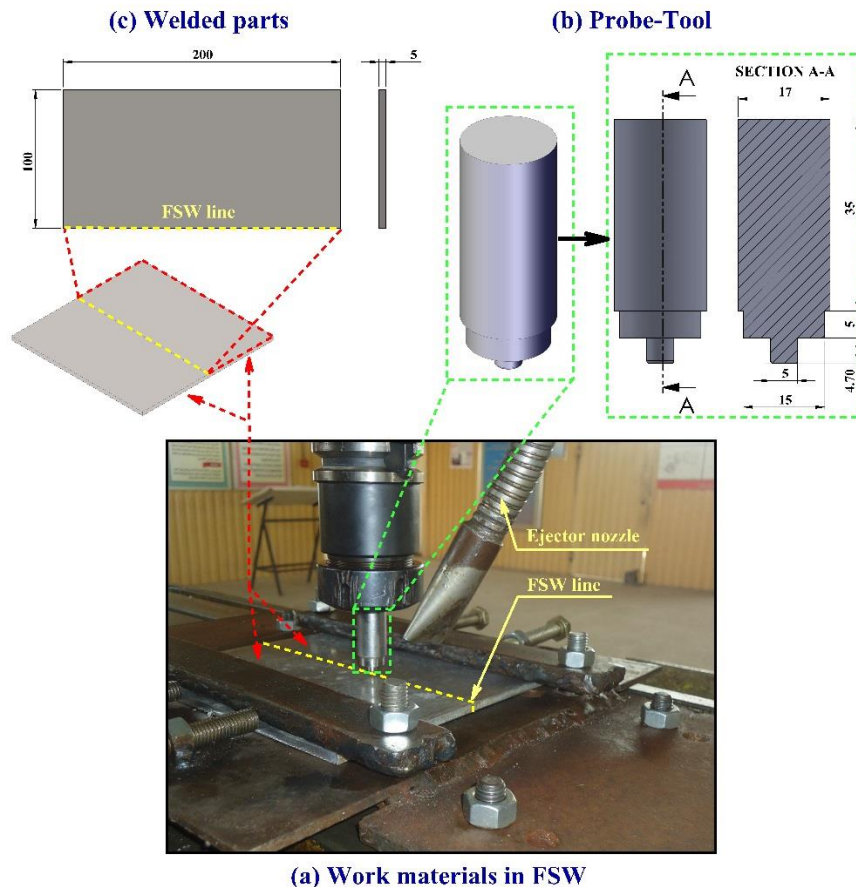


Figure 1. FSW environment to weld AA2024-T3: (a) Work materials, (b) Probe-Tool dimensions, (c) Welded parts dimensions

After tensile samples were being prepared by the Wire-EDM machine (Model: DK7732-SUNDA, China), each specimen was fixed in the testing machine (Model: WDW Series-Beijing United Test, China). In Figure 3(a), the fixing status of the specimen was shown in this testing machine. Moreover, the ASTM-B557M standard was used with each sample, as depicted in Figure 3(b). Therefore, this testing machine is responsible for specifying ultimate tensile strength (TS) and the ratio of tensile strength efficiency (%TSE), as functions in the present study. Accordingly, this study has reported the influence of the natural flow of air besides ejected air and water on these tensile functions.

As aforementioned, these functions are considered as the responses to determine the optimum performance of tensile samples. Here, this performance has wholly resulted from these flow mechanisms of air and water.

3. Experimental design and optimization

The experimental conditions of the FSW medium are very significant to control the performance of rectangular parts welding of AA 2024-T3, as clarified in Figure 1(a) and (c). Hence, these conditions can be divided into two kinds: fixed as feeding rate and nozzle pressure. Meanwhile, the other conditions are variable behaviors on the experimental side, as demonstrated in Table 1. Therefore, flow mechanism (FM) and rotational speed (RS) were considered variable conditions. In other words, these conditions were applied as variable parameters in this medium.

Depending on Table 1, the influential parameters' levels were observably adopted to design the experimental runs. These runs were devised employing General Full Factorial (GFF) technique in the present study. Hence, the models in Eqs. (1) and (2) reflect the essential and polynomial equations employed to fit and predict the experimental values of responses. Consequently, ultimate tensile strength (TS) and the ratio of tensile strength efficiency (%TSE) represent these responses resulting from the fracture case of each sample at each run.

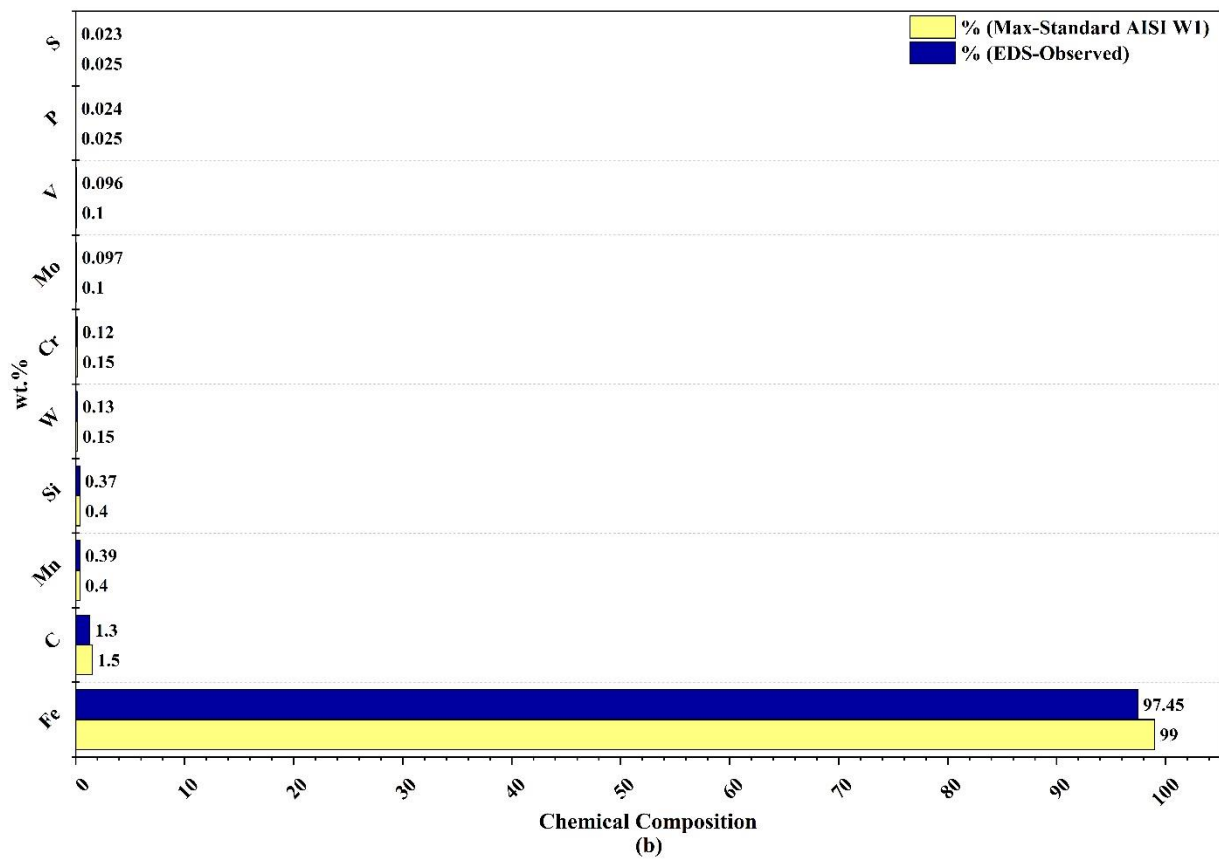
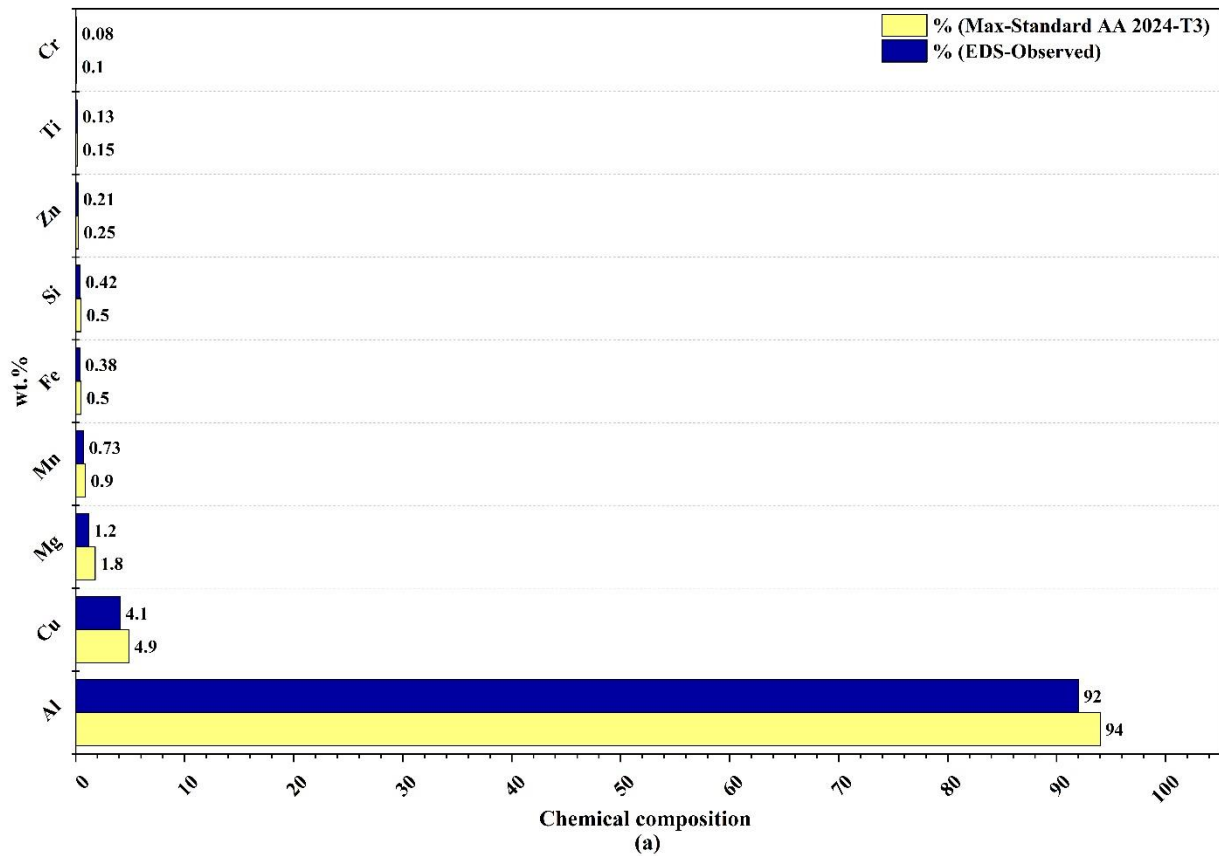
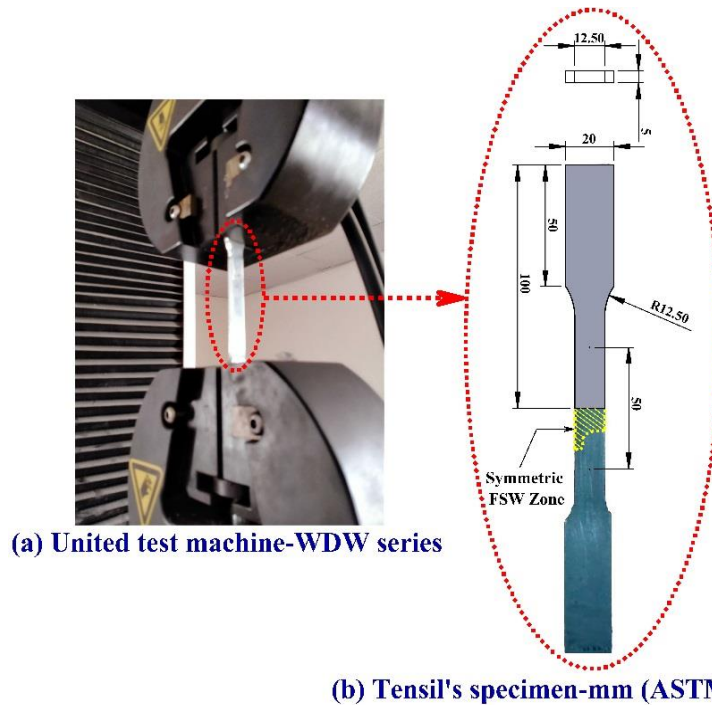


Figure 2. Chemical composition comparison among standard and EDS-Observed of (a) Workpiece: AA 2024-T3, (b) Probe-Tool: Water Hardening Tool Steel AISI W1



(a) United test machine-WDW series

(b) Tensile's specimen-mm (ASTM-B557M)

Figure 3. Tensile test environment. Notes: (a) Fixing tensile sample in United test machine-WDW series; (b) Specimen standard-mm according to ASTM-B557M

Table 1. Variable parameters' levels utilized in the experimental optimization

Variable parameter	Code	Levels		
		-1	0	+1
Rotational speed (rpm)	RS	800	1000	1200
Flow mechanism	FM	Natural air (NA)	Forced air (FA)	Forced water (FW)

$$E_r = nL^P, \tag{1}$$

$$R = A_0 + A_1X_{-1} + A_2X_0 + A_3X_1 + A_4Y_{-1} + A_5Y_0 + A_6Y_1 + A_7X_{-1}Y_{-1} + A_8X_{-1}Y_0 + A_9X_{-1}Y_1 + A_{10}X_0Y_{-1} + A_{11}X_0Y_0 + A_{12}X_0Y_1 + A_{13}X_1Y_{-1} + A_{14}X_1Y_0 + A_{15}X_1Y_1, \tag{2}$$

where E_r indicates the total of experimental runs, L is the levels of each parameter, n is the replicates number of corner points, and P is the number of variable parameters. On the other hand, R refers to the response, A is the coefficient of regression, while X and Y are RS and FM, respectively. Thus, the whole number of the experimental runs applied in the present work is 18. In Table 2, the number of runs and the values of these responses at each run were demonstrated.

The criterion adopted in this study for responses TS and %TSE were *larger-the-better* (LB) of desirability function for optimizing the multi-objective. Therefore, the statistical medium Minitab 18 was employed to implement the analysis and optimization of these responses. Hence, the desirability function (D) as composite value for this multi-objective can be seen in Eqs. (3) and (4) [16], [17], [18], [19], [20]:

$$d_k(R) = \begin{cases} 0 & R_n < L_n \\ \left[\frac{R_n - L_n}{T_n - L_n} \right]^w & L_n \leq R_n < T_n \\ 1 & R_n > T_n \end{cases} \tag{3}$$

$$D = (d_1 \cdot d_2 \cdot \dots \cdot d_k)^{1/k}, \tag{4}$$

Table 2. Experimental design and outcomes of responses TS and %TSE

Runs No.	RS (RPM)	FM	TS (MPa)	FIT*	RES†	%TSE	FIT	RES
1	-1	-1	198	196.5	1.5	43	45.5	2.5
2	-1	0	220	223.0	3.0	45	45.5	0.5
3	-1	1	235	232.5	2.5	48	49.0	1.0
4	0	-1	240	242.5	2.5	52	53.5	1.5
5	0	0	257	258.5	1.5	55	56.0	1.0
6	0	1	290	291.5	1.5	63	61.5	1.5
7	1	-1	224	222.0	2.0	48	48.5	0.5
8	1	0	260	263.0	3.0	58	59.0	1.0
9	1	1	300	298.0	2.0	68	69.0	1.0
10	-1	-1	195	196.5	1.5	48	45.5	2.5
11	-1	0	226	223.0	3.0	46	45.5	0.5
12	-1	1	230	232.5	2.5	50	49.0	1.0
13	0	-1	245	242.5	2.5	55	53.5	1.5
14	0	0	260	258.5	1.5	57	56.0	1.0
15	0	1	293	291.5	1.5	60	61.5	1.5
16	1	-1	220	222.0	2.0	49	48.5	0.5
17	1	0	266	263.0	3.0	60	59.0	1.0
18	1	1	296	298.0	2.0	70	69.0	1.0

*FIT: Fitting of experimental values; †RES: Residual among experimental and fit values.

where $d_k(R)$ is a sub-desirability function based on LB-Criterion of desired response R_n , while L_n and T_n are the lower limit of desired response and desired target for the response, sequentially. In addition, w and k are the weight factor and responses number, individually. Currently, the weight w applied to specify D in this multi-objective optimization equals one.

This concise description has presented a whole concept of the design and optimization of the existing experimental environment. Therefore, the scenario of this environment contributes to analyzing, discussing, and interpreting the outcomes in Table 2. Moreover, these outcomes lead to selecting the optimal run for TS and %TSE.

4. Results and discussion

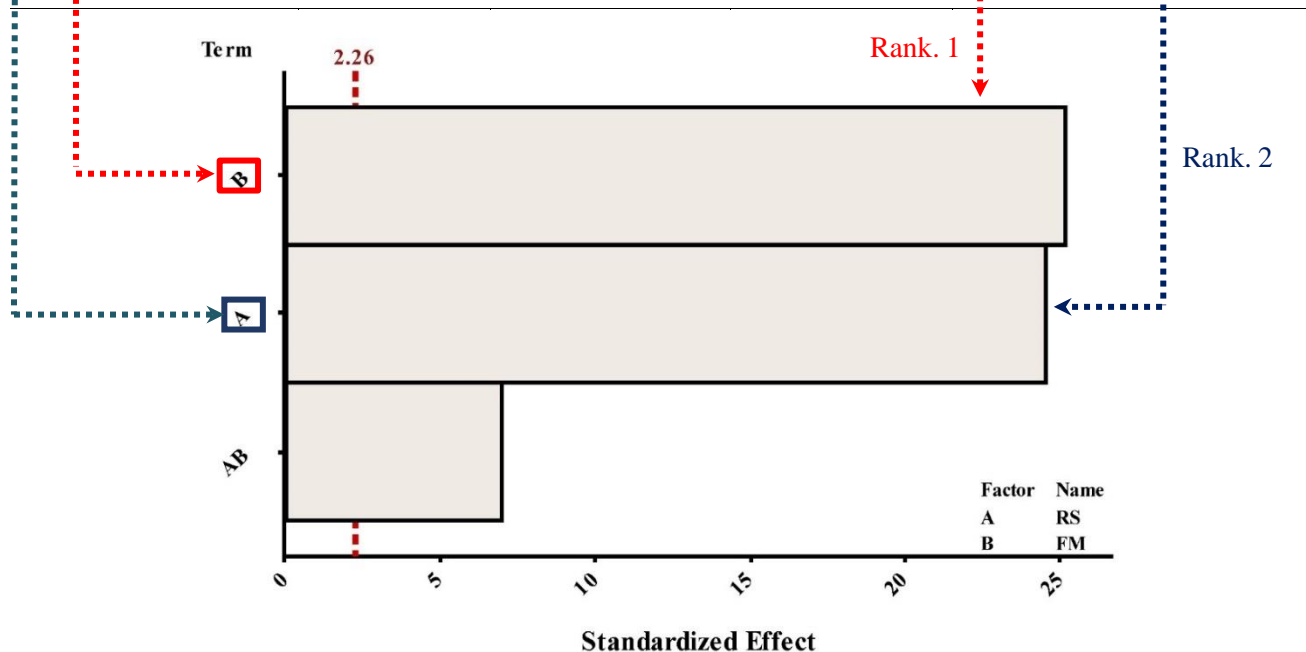
The statistical analysis is considered a pointer to specify the significant parameters of TS and %TSE responses depending on P-Values and F-Values. Accordingly, these values as outputs to Analysis of Variance (ANOVA) are computed based on the values of these responses exhibited in Table 2. In turn, the values of FIT and RES were observed as a preliminary evaluation of outcomes. Thus, the RES values are (1.5-3) and (1-2.5) in Table 2 for TS and %TSE, respectively.

In Table 2, the concrete results of FIT and RES led to boosting the experimental responses to be beneficial to conduct the ANOVA. Thus, this means identifying the vital parameters of TS and %TSE in the present research [21], [22], [23]. The outcomes of ANOVA of TS were significant to the linear states: RS and FM, besides the interacted case: RS×FM since the P-Values of these cases were <5%, as illustrated in Table 3 [24].

Furthermore, the F-Value and chart of Pareto's effect in Table 3 as an index reflect the parameters rank of this study. According to this index, both FM and RS were first and second, respectively. In addition, the interacted case RS×FM was third depending on the ultimate TS outcomes. Thus, the flow mechanism has boosted the ultimate tensile strength, although the rotational speed contributed to this enhancement. Hence, the outputs of ANOVA for TS of specimen produced by FSW of AA 2024-T3 in the current work corresponded to this behavior [13], [25]. Moreover, the regression model in Eq. (5), as a polynomial form of TS, fitted and correlated with experimental outcomes, where the correlation factors of this model were 99.5%, 99.05%, and 97.99% for R-sq, R-sq(adj), and R-sq(pred), correspondingly.

Table 3. ANOVA and chart of Pareto's effect for TS

Source	DOF [#]	Adj-SS [*]	Adj-MS [†]	F-Value [‡]	P-Value [‡]
Model	8	17898.0	2237.25	222.49	0.000
Linear	4	16864.7	4216.17	419.29	0.000
RS	2	8220.3	4110.17	408.75	0.000
FM	2	8644.3	4322.17	429.83	0.000
Interactions	4	1033.3	258.33	25.69	0.000
RS×FM	4	1033.3	258.33	25.69	0.000
Error	9	90.5	10.06		
Total	17	17988.5			



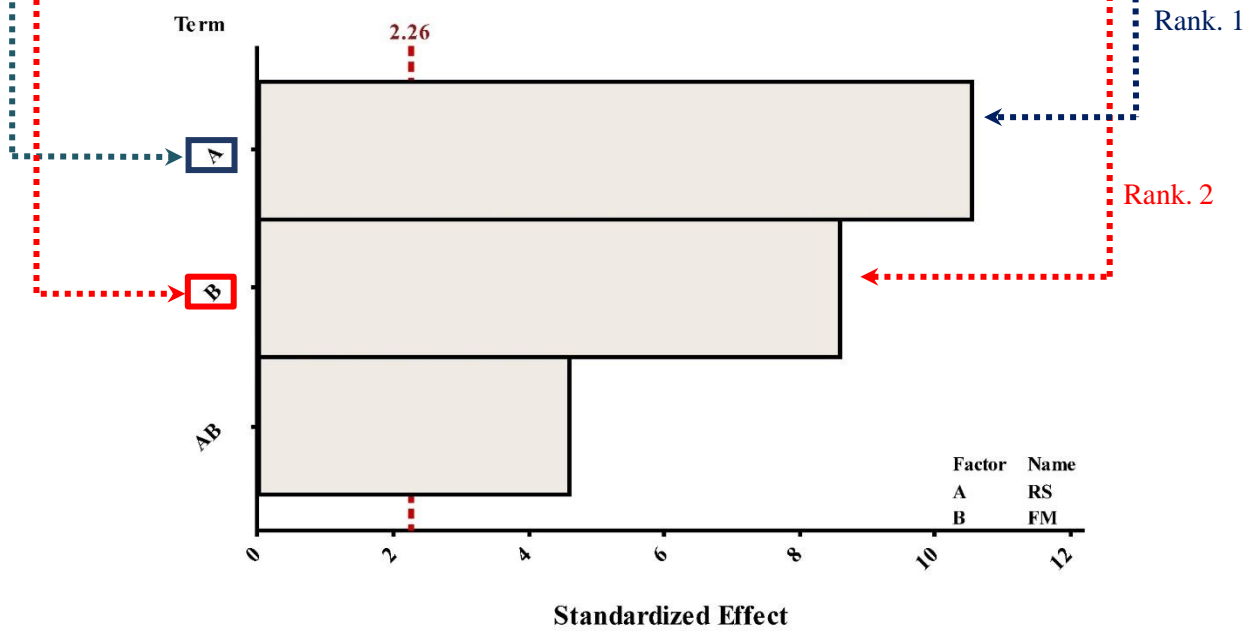
#DOF: Degree of freedom; *Adj-SS: Adjusted summation squares related to factor variation in the model; †Adj-MS: Adjusted mean squares related to factor variation in the model; ‡F-Value: Standard ratio with the greatest value to specify the important values in ANOVA; ‡P-Value: Standard ratio with the stable values (0 ≤ P-Value ≤ %5) to specify an important value in ANOVA.

$$\begin{aligned}
 TS = & 247.5 - 30.17RS_{-1} + 16.67RS_0 + 13.5RS_1 - 27.17FM_{-1} + 0.67FM_0 + 26.5FM_1 \\
 & + 6.33RS_{-1}FM_{-1} + 5RS_{-1}FM_0 - 11.33RS_{-1}FM_1 + 5.5RS_0FM_{-1} - 6.33RS_0FM_0 \quad (5) \\
 & + 0.83RS_0FM_1 - 11.83RS_1FM_{-1} + 1.33RS_1FM_0 + 10.5RS_1FM_{-1}.
 \end{aligned}$$

On the contrary, ANOVA results of %TSE clarified that the rank of RS and FM are first and second, depending on F-Value and chart of Pareto's effect, sequentially. Meanwhile, P-Values were < 5% for RS, FM, and RS×FM, in which these values were significant, as depicted in Table 4. Additionally, the regression model for %TSE in Eq. (6) reflects the sobriety of statistical analysis performance of %TSE. This sobriety performance can be seen by the correlation factors R-sq, R-sq(adj), and R-sq(pred). Moreover, the values of these factors were 97.1%, 94.52%, and 88.39%. The decrease of the rotational speed of Probe-Tool plays a notable role in dropping the ratio of tensile strength efficiency of the sample under the tensile test [26]. However, it did not supply research evidence about the relation among %TSE response and the influence of flow mechanism (FM) in FSW, like the evidence available amongst TS and FM. Therefore, with the loss of this evidence, it is difficult to recognize the dominant parameter among RS and FM in this response. Consequently, the ANOVA for %TSE in Table 4 has presented novel outcomes demonstrating RS as a dominant parameter.

Table 4. ANOVA and chart of Pareto's effect's for %TSE

Source	DOF	Adj-SS	Adj-MS	F-Value	P-Value
Model	8	1020.00	127.500	37.62	0.000
Linear	4	861.67	215.417	63.57	0.000
RS	2	516.33	258.167	76.18	0.000
FM	2	345.33	172.667	50.95	0.000
Interactions	4	158.33	39.583	11.68	0.001
RS×FM	4	158.33	39.583	11.68	0.001
Error	9	30.50	3.389		
Total	17	1050.50			



$$\begin{aligned}
 \%TSE = & 54.167 - 7.5RS_{-1} + 2.833RS_0 + 4.667RS_1 - 5FM_{-1} - 0.667FM_0 + 5.667FM_1 \\
 & + 3.833RS_{-1}FM_{-1} - 0.5RS_{-1}FM_0 - 3.333RS_{-1}FM_1 + 1.5RS_0FM_{-1} \\
 & - 0.333RS_0FM_0 - 1.167RS_0FM_1 - 5.333RS_1FM_{-1} + 0.833RS_1FM_0 \\
 & + 4.5RS_1FM_{-1}.
 \end{aligned} \tag{6}$$

The outputs of ANOVA for TS and %TSE have illustrated the significant role of FM to TS and RS to %TSE, as the topped influential parameters, in the performance of FSW of AA 2024-T3. However, this analysis did not specify the impacting level of RS and FM as a pivotal job. Hence, this job can be implemented by adopting Eqs. (3) and (4) as multi-objective optimization. Additionally, the weight factor (w) employed in Eq. (3) is equal to one. As a result, the optimal predicted parameters can be recognized in Table 5 and Figure 4. Hence, these parameters were 1200 rpm and forced water (FW) for rotational speed and flow mechanism, severally. Furthermore, the composite desirability (D) is 0.9719 for the multi-objective optimization of TS and %TSE. On the other hand, both the experimental runs No. 9 and 18 have referred to the optimal runs since the parameters in each run are consistent with the optimal parameters. Besides, the residual values between predicted and experimental outcomes for TS and %TSE were 2 and 1, sequentially.

Table 5. Predicted and experimental outcomes of TS and %TSE utilizing Optimal parameters

Optimal predicted parameters		Valid run	TS (MPa)		
RS (RPM)	FM		Predicted outcome	Experimental outcome	RES
1200	FW	9	298	300	2
		18	298	296	2
		Valid run	%TSE		
			Predicted outcome	Experimental outcome	RES
		9	69	68	1
		18	69	70	1

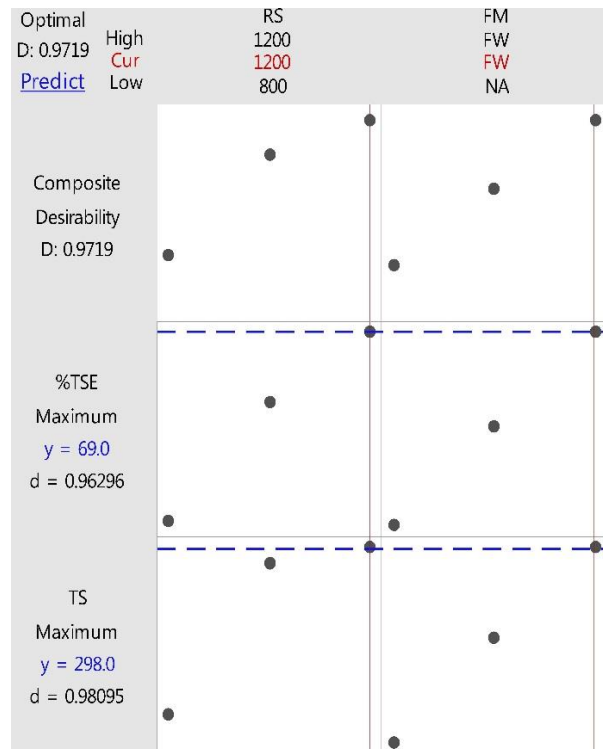


Figure 4. Multi-Objective optimization and composite desirability for TS and %TSE

The increasing rotational speed up to 1200 rpm contributes to growing the generated temperature by FSW operation. Thereby, the heat deeply expands to penetrate the base material zone (BMZ) and enlarge the Heat

Affected Zone (HAZ) depending on the recrystallization phenomenon and growth of the grains size [25], [27], [28]. Nevertheless, the water-cool leads to efficient control in enhancing the strength of the Welding Joint Zone (WJZ) by reducing this penetration and reducing the grains' size. Besides, the water-cool diminishes the nugget region to produce minimal corrosion of WJZ [13], [29]. Thus, the multi-objective optimization outputs induced from the present work is compatible with this interpretation.

To confirm the optimal outputs in Table 5 and Figure 4, the morphology of the fracture zone in Figure 5(a)-(c) can be observed under magnification 200 μm and 20 μm for 2D and 3D-SEM-Micrograph of run No. 9. In Figure 5(b) and (c), the distribution of big dimples was an indicator of high ductile and plastic deformation of the fracture zone [30]. By contrast, Figure 5(d)-(f) refers to the brittle fracture in run No. 10 as a worst-case among 18 runs based on the minimal criterion value of the ultimate tensile strength illustrated in Table 2. Observably, the distribution of voids as described in Figure 5(e) and (f) in the morphology of the fracture zone is the primary reason for the brittleness in this run [25].

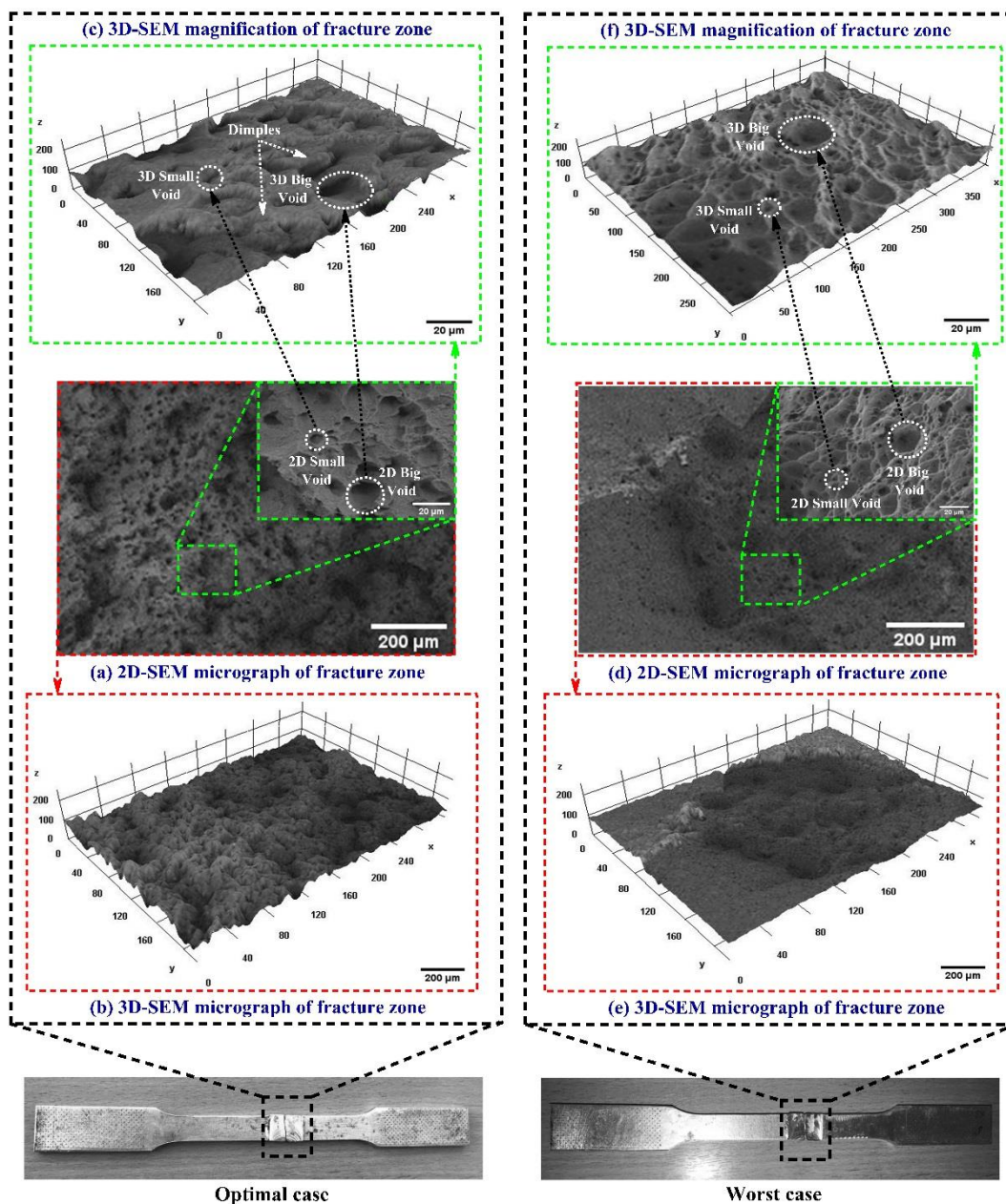


Figure 5. 2D and 3D SEM-Micrograph of fracture zone: Optimal case(a)-(c) under run No. 9; Worst case (d)-(f) under run No. 10

These encouraging findings of FSW on AA 2024-T3 had revealed the character of forced water, as an active convection case, in limiting the growth of grains size at high rotational speed to boosting TS and %TSE. Hence, this study proved that the statistical analysis and multi-objective optimization techniques have contributed to understanding the role of this convection in presenting a logical performance.

5. Conclusions

The present work has utilized air and water ejected, besides the natural air as boundary conditions under 800, 1000, and 1200 rpm, as the rotational speed in the FSW of AA 2024-T3. Hence, it has remarkably concluded to the following outputs:

1200 rpm and forced water are considered an optimal rotational speed and flow mechanism to implement FSW of AA 2024-T3 relying on Multi-Objective Optimization using GFF technique. Consequently, the fracture zone morphology under these optimal parameters had contained large dimples distributed along this zone. Therefore, these dimples' size has reversed the efficient performance of plastic deformation. Moreover, it was enhanced the strength of the welding-joint-zone.

Acknowledgements

The authors would like to express their profound gratitude and deepest appreciation to the Ministry of Higher Education and Scientific Research, Iraq. Furthermore, the authors would like to express their special thanks to Sustainable Manufacturing and Recycling Technology-Advanced Manufacturing and Materials Centre (SMART-AMMC), Universiti Tun Hussein Onn Malaysia (UTHM), Malaysia, besides Kut Technical Institute, Middle Technical University, and Engineering Technical College-Najaf, Al-Furat Al-Awsat Technical University (ATU), Iraq, for their support.

Conflict of interest On behalf of all authors, the corresponding author declares no conflict of interest.

References

- [1] A. Kubit, D. Wydrzynski, M. Bucior and B. Krasowski, "Testing of stiffening ribs formed by incremental forming in thin-walled aircraft structures made of 2024-T3 Alclad aluminium alloy," *AIP Conf. Proc.*, vol. 1960, no. 1, p. 160015, 2018.
- [2] K. Jones and DW. Hoepfner, "Prior corrosion and fatigue of 2024-T3 aluminium alloy," *Corros Sci*, vol. 48, no. 10, pp. 3109-22, 2006.
- [3] G. Peng, Q. Yan, J. Hu, P. Chen, Z. Chen and T. Zhang, "Effect of forced air cooling on the microstructures, tensile strength, and hardness distribution of dissimilar friction stir welded AA5A06-AA6061 joints," *Metals (Basel)*, vol. 9, no. 3, P. 304, 2019.
- [4] P. Patel, H. Rana, V. Badheka, V. Patel and W. Li, "Effect of active heating and cooling on microstructure and mechanical properties of friction stir-welded dissimilar aluminium alloy and titanium butt joints," *Weld World*, vol. 64, no. 2, pp. 365-78, 2020.
- [5] AS. Franchim, FF. Fernandez and DN. Travessa, "Microstructural aspects and mechanical properties of friction stir welded AA2024-T3 aluminium alloy sheet," *Mater Des*, vol. 32, no. 10, pp. 4684-8, 2011.
- [6] T. Ghorbanzade, A. Soltanipour, K. Dehghani and A. Chabok, "Microstructural evolutions and mechanical properties of friction stir welded AA2024-3," *Proc Inst Mech Eng Part L J Mater Des Appl*, vol. 230, no. 1, pp. 75-87, 2016.
- [7] D. Trimble, GE. O'Donnell and J. Monaghan, "Characterisation of tool shape and rotational speed for increased speed during friction stir welding of AA2024-T3," *J Manuf Process*, vol. 17, no. January, pp. 141-50, 2015.
- [8] N. Li, W. Li, Y. Xu, X. Yang and ND. Alexopoulos, "Influence of rotation speed on mechanical properties and corrosion sensitivity of friction stir welded AA2024-T3 joints," *Mater Corros*, vol. 69, no. 8, pp. 1016-24, 2018.

- [9] P. Carlone and GS. Palazzo, "Experimental analysis of the influence of process parameters on residual stress in AA2024-T3 friction stir welds," *Key Eng. Mater.*, vol. 504, no. February, pp. 753-8, 2012.
- [10] P. Carlone and GS. Palazzo, "Longitudinal residual stress analysis in AA2024-T3 friction stir welding," *Open Mech Eng J*, vol. 7, no. 1, pp. 18-26, 2013.
- [11] B. Bagheri, M. Abbasi and M. Dadaei, "Effect of water cooling and vibration on the performances of friction-stir-welded AA5083 aluminium joints," *Metallogr Microstruct Anal*, vol. 9, no. 1, pp. 33-46, 2020.
- [12] TS. Rao, SRK. Rao and GM. Reddy, "Microstructure and Fracturing Behavior of AA7075-T651 Aluminium Alloy Cooled During Friction Stir Welding," *Met Sci Heat Treat*, vol. 61, no. 5, pp. 379-86, 2019.
- [13] S. Sinhmar and DK. Dwivedi, "Enhancement of mechanical properties and corrosion resistance of friction stir welded joint of AA2014 using water cooling," *Mater Sci Eng A*, vol. 684, no. January, pp. 413-22, 2017.
- [14] S. Balaji, B. Sujay Aadithya and K. Balachandar, "Conventional and underwater friction stir welded AA2024-T351 aluminium alloy-a comparative analysis," *World J Eng*, vol. 17, no. 6, pp. 795-801, 2020.
- [15] MA. Abbas, "Agglomeration Phenomenon in Machining of AISI D2 Hardened Steel Using Chromium Powder Mixed-EDM," *Universiti Tun Hussein ONN Malaysia (UTHM)*, pp. 186-187, 2020.
- [16] G. Derringer and R. Suich, "Simultaneous optimization of several response variables," *J Qual Technol*, vol. 12, no. 4, pp. 214-9, 1980.
- [17] E. Del Castillo, DC. Montgomery and DR. McCarville, "Modified desirability functions for multiple response optimization," *J Qual Technol*, vol. 28, no. 3, pp. 337-45, 1996.
- [18] MA. Abbas, MA. Lajis, AD. Jawad, EA. Rahim, S. Ahmed and NA. Jamil, "Influence of the spark heat on the electrode behavior in Powder Mixed-EDM environment," *J Mech Eng Sci*, vol. 13, no. 4, pp. 6125-43, 2019.
- [19] A. Fitrianto and H. Midi, "Multi-Response Optimization via Desirability Function for the Black Liquor DATA," *J Sci Technol*, vol. 4, no. 1, pp. 90-101, 2012.
- [20] GC. Derringer, "A balancing act-optimizing a product's properties," *Qual Prog*, vol. 27, no. 6, pp. 51-8, 1994.
- [21] EM. Sefene and AA. Tsegaw, "Temperature-based optimization of friction stir welding of AA 6061 using GRA synchronous with Taguchi method," *Int J Adv Manuf Technol*, no. November, pp. 1-12, 2021.
- [22] A. Mahdianikhotbesara, MH. Sehhat and M. Hadad, "Experimental study on micro-friction stir welding of dissimilar butt joints between Al 1050 and pure copper," *Metallogr Microstruct Anal*, vol. 10, no. 4, pp. 458-73, 2021.
- [23] GSVS. Kumar, A. Kumar, S. Rajesh, RBR. Chekuri and VP. Sundaramurthy, "Experimental and thermal investigation with optimization on friction stir welding of nylon 6A using Taguchi and microstructural analysis," *Adv Mech Eng*, vol. 13, no. 10, p. 16878140211050737, 2021.
- [24] Sachinkumar, D. Chakradhar and S. Narendranath, "Analysis of the Effect of Friction Stir Welding Parameters on Characteristics of AA6061 Composites using Response Surface Methodology," *Trans Indian Inst Met*, no. March, pp. 1303-1319, 2021.
- [25] HJ. Zhang, HJ. Liu and L. Yu, "Microstructure and mechanical properties as a function of rotation speed in underwater friction stir welded aluminium alloy joints," *Mater & Des*, vol. 32, no. 8-9, pp. 4402-7, 2011.
- [26] S. Balos and L. Sidjanin, "Effect of tunneling defects on the joint strength efficiency obtained with FSW," *Mater Technol*, vol. 48, no. 4, pp. 491-6, 2014.
- [27] A. Astarita, A. Squillace and L. Carrino, "Experimental study of the forces acting on the tool in the friction-stir welding of AA 2024 T3 sheets," *J Mater Eng Perform*, vol. 23, no. July, pp. 3754-61, 2014.
- [28] R. Fu, J. Zhang, Y. Li, J. Kang, H. Liu and F. Zhang, "Effect of welding heat input and post-welding natural aging on the hardness of stir zone for friction stir-welded 2024-T3 aluminium alloy thin-sheet," *Mater Sci Eng A*, vol. 559, no. January, pp. 319-24, 2013.

- [29] SS. Sabari, S. Malarvizhi and V. Balasubramanian, "Influences of tool traverse speed on tensile properties of air-cooled and water-cooled friction stir welded AA2519-T87 aluminium alloy joints," *J Mater Process Technol*, vol. 237, no. November, pp. 286–300, 2016.
- [30] B. Robitaille, PR. Provencher, L. St-Georges and M. Brochu, "Mechanical properties of 2024-T3 AlClad aluminium FSW lap joints and impact of surface preparation," *Int J Fatigue*, vol. 143, no. February, p. 105979, 2021.